



Cite this: DOI: 10.1039/c7ta10575d

Received 1st December 2017  
Accepted 22nd February 2018

DOI: 10.1039/c7ta10575d

rsc.li/materials-a

## A novel Ru–polyethersulfone (PES) catalytic membrane for highly efficient and selective hydrogenation of furfural to furfuryl alcohol†

G. Bagnato,<sup>a</sup> A. Figoli,<sup>b</sup> C. Ursino,<sup>b</sup> F. Galiano<sup>b</sup> and A. Sanna<sup>a\*</sup>

A novel catalytic membrane has been synthesised, characterised and evaluated for the selective hydrogenation of furfural to furfuryl alcohol. Unlike conventional methods, involving high pressure and high H<sub>2</sub> : feed ratios, this work proposes an innovative ruthenium based Catalytic Membrane Reactor (CMR) to overcome mass transfer limitations, resulting in low H<sub>2</sub> requirements, high catalytic activity and high selectivity towards furfuryl alcohol. A UV-curable hydrophilic anionic monomer acrylic acid was used as a coating material on a commercial PES membrane and subsequently Ru nanoparticles were added. The hydrogenation of furfural was carried out in a customised catalytic membrane reactor under mild conditions: 70 °C and 7 bar, exhibiting high catalytic activity towards furfuryl alcohol (selectivity >99%) with turnover frequency (TOF) as high as 48 000 h<sup>-1</sup>, 2 orders of magnitude higher than those obtained so far.

The production of bio-fuels or chemicals from biomass derivatives, such as by pyrolysis/liquefaction of bio-oils or cellulose hydrolysis, is a promising pathway to reduce the dependence on fossil fuels and reduce the emission of greenhouse gases. Bio-oils are obtained by fast pyrolysis of lignocellulosic biomass, marine biomass and bio-waste.<sup>1,2</sup> Bio-oil is a dark brown liquid with high viscosity and high oxygen and water contents, which limit its use as a fuel in common engines. To decrease the oxygen content and convert highly reactive functionalities into more stable ones, bio-oils can be subjected to hydrogenation reactions<sup>3–6</sup> resulting in compounds with a higher economic value that can be used for the production of polymers, cosmetics, food additives or drop-in fuels. Furfuryl alcohol is an important chemical intermediate for the production of chemical products, such as vitamin C, lysine, plasticizers, dispersing

agents and lubricants.<sup>7</sup> Furfuryl alcohol can be manufactured by the chemoselective hydrogenation of furfural, which is an aldehyde with a heterocyclic structure and a common product of lignocellulose pyrolysis and/or cellulose hydrolysis.<sup>8–10</sup> The production of furfuryl alcohol from renewable sources has recently attracted great interest.

Furfural is mainly derived from a variety of agricultural products, including corn, oats, wheat, bran and sawdust. Industrially, the hydrogenation of furfural is used to obtain furfuryl alcohol, an intermediate product for the industrial production of resin.<sup>11</sup> Fig. 1 shows the reaction pathway for the hydrogenation of furfural. Furfuryl alcohol formation is in competition with tetrahydrofurfural formation *via* the saturation of different functional groups, aldehyde and the heterocyclic group, respectively.

Other undesirable products derived from the hydrogenation/dehydration of furfural are 2 methylfuran, 2 methyltetrahydrofuran on further hydrogenation and pentanol on consecutive hydrogenation. Furthermore, decarbonylation reactions are favoured under the same conditions of the hydrogenation reaction, leading to the formation of furan and subsequently, butanol.<sup>12</sup> All these competing reactions render it difficult to control the selectivity of the desired product.

The hydrogenation of furfural has been studied in both gas and liquid phases,<sup>13–15</sup> in the presence of metal catalysts, in particular the elements of IX (Co, Rh, and Ir) and X (Ni, Pt, and Pd) groups and Cu, on supports such as SiO<sub>2</sub>, C or Al<sub>2</sub>O<sub>3</sub>.<sup>13,16–19</sup>

O'Driscoll *et al.*<sup>20</sup> synthesized a Pt–Sn/SiO<sub>2</sub> catalyst to study furfural hydrogenation at different reaction temperatures between 25 and 150 °C at 20 bar and with different solvents in a batch reactor. The authors obtained a complete conversion after 48 h at 100 °C in the presence of toluene. Chen *et al.*<sup>14</sup> achieved a complete conversion after 5 h at 100 °C and 10 bar in the presence of Pt supported on g-C<sub>3</sub>N<sub>4</sub>. Rh and Pt nanoparticles stabilized by phosphine-functionalized silica were studied by Llop *et al.* for the hydrogenation of different bio-oil compounds.<sup>21</sup> At 80 °C and 40 bar, furfural was completely converted into furfuryl alcohol in the presence of Pt, while the conversion was about 16% using Rh.

<sup>a</sup>Institute of Mechanical, Process and Energy Engineering, School of Engineering & Physical Sciences, Heriot-Watt University, Edinburgh EH14 4AS, UK. E-mail: a.sanna@hw.ac.uk

<sup>b</sup>Institute on Membrane Technology (ITM-CNR), Via P. Bucci, 17/c, I-87030 Rende, CS, Italy

† Electronic supplementary information (ESI) available. See DOI: 10.1039/c7ta10575d

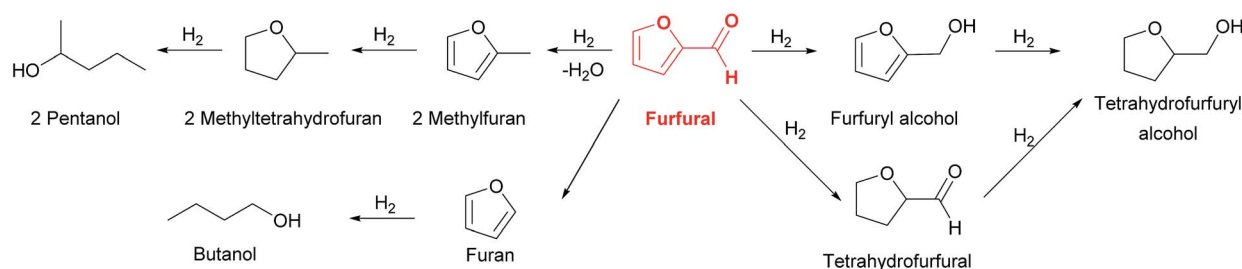


Fig. 1 Reaction pathways.

The above studies indicate that a high pressure (>10 bar) and/or long residence time (hours) are required for the successful selective conversion of furfural into furfuryl alcohol, using traditional reactors (continuous and batch). The main disadvantage of hydrogenation reactions is represented by the mass transport limitation, due to the reactions taking place in gaseous, liquid and solid phases. The system must operate under high pressure, which improves the gas solubility in the liquid system, and at high temperature, which benefits the kinetics. However, the hydrogen solubility decreases under those conditions. The choice of reaction temperature and pressure is dictated by the conversion of the limiting reagent and the selectivity of the desirable product. With the purpose of overcoming the mass transfer limitation, the use of a membrane reactor (MR) represents a valid choice.<sup>22–24</sup> According to the IUPAC definition, a MR is a device for simultaneously carrying out a reaction and a membrane-based separation, in the same physical enclosure.<sup>25</sup> The membrane can have extractor, distributor or active layer functionalities. For example, Bagnato *et al.*<sup>26</sup> used a dense Pd–Ag membrane to extract H<sub>2</sub> from the reaction zone during the steam reforming of a model bio-ethanol in the presence of the Ni/CeO<sub>2</sub> catalyst. They compared the performance of a MR and a packed bed reactor (PBR) at 400 °C, at a gas hourly space velocity (GHSV) of 800 h<sup>-1</sup>, obtaining the best conversion and hydrogen yield by using the MR. Catalytic membrane reactors were recently proposed for the conversion of biomass substrates into bio-chemicals. The hydrogenation of levulinic acid was carried out using a porous expanded polytetrafluoroethylene (ePTFE) membrane with Ru catalyst particles by Stanford *et al.*<sup>27</sup> Different membranes, with and without a dense Matrimid layer, were tested to evaluate the hydrogen flux through them. The hydrogenation reaction was studied in the reaction temperature and pressure range of 40–90 °C and 0.7–5.6 bar, respectively. Furthermore, the authors compared the results obtained with a PBR considering the kinetic rate of the gamma-valerolactone product over grams of Ru. The MR without the Matrimid layer resulted in the best performance (rate was 4 times higher than that of the PBR), but with a low conversion of 0.0065%, while the MR with the control layer (Matrimid) showed a kinetic rate 2 times lower than that of the PBR. Two different MRs were studied by Liu *et al.*,<sup>28</sup> who compared (i) a MR plus a catalytic packed bed, where the membrane acted as a H<sub>2</sub> distributor in the reaction zone (where the catalyst was allocated) and (ii) a catalytic MR, where the membrane was modified by adding a catalytic layer. The two systems were tested for the

hydrogenation of nitrobenzene in the presence of the Pd/γ-Al<sub>2</sub>O<sub>3</sub> catalyst. The authors noted that the membrane with the catalytically active layer showed the best performance in terms of conversion and catalytic stability, ~85% for 10 hours. Instead, the MR with the separate catalytic packed bed achieved a conversion of about 20% and 60%, respectively, after 4 and 6 hours. A limited number of studies have been focused on the specific catalytic hydrogenation of furfural and all of them were done using batch reactors.<sup>14,16,17</sup> The outcomes of these studies are discussed and compared to the findings of this work in the last part of this work. The aim of this work was to develop and test a novel catalytic membrane reactor in order to selectively hydrogenate bio-oil derived compounds by reducing the amount of hydrogen used. To the best of our knowledge, Ru-functionalised PES membranes have never been synthesized and tested for hydrogenation reactions. Recently, Mengistie *et al.*<sup>29</sup> used a Pd–PES membrane for the hydrogenation of the –NO<sub>2</sub> group in nitrophenol in a flow-through catalytic membrane reactor, denoting the stability of PES as a support for Pd.

In this work, a novel catalytic membrane with an active layer was synthesised by modifying a commercial PES membrane by photochemical graft<sup>30,31</sup> polymerization of acrylic acid and doping its surface with Ru nanoparticles. The modified membrane was characterized in terms of morphology, porosity, pore size diameter, contact angle and Ru content. After that, the catalytic membrane was tested for the hydrogenation of furfural under mild process conditions for evaluating its turnover frequency (TOF). The commercial PES membranes (supplied from Hangzhou Cobetter Filtration Equipment Co., China), with different pore sizes (from 50 to 800 nm), were dipped in a grafting solution composed of 25 wt% acrylic acid, 2.83 wt% *N,N'*-methylene-bisacrylamide and 0.0753 wt% 4-hydroxybenzophenone in water. The PES membrane exposed to UV light (two lamps from General Electric, UV output: 2.2 watt, gap from the samples: 6 cm), and in the presence of photoinitiators, led to the dissociation of free radicals with consecutive polymerization of acrylic acid on the membrane surface.

The irradiation time was between 5 and 30 min, equivalent to 4.84–14.53 J cm<sup>-2</sup> energy flux. Subsequently, the grafted membranes were washed with distilled water to remove the excess grafting solution and dried. The modified PES membrane was dipped in hexaammine-ruthenium(II) chloride solution (0.01 M) for 18 hours at room temperature.<sup>29</sup> The solution reacted with the carboxyl group of acrylic acid on the PES membrane (Fig. 2).

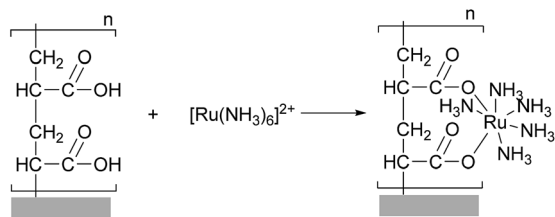


Fig. 2 Precursor loading.

A  $\text{Na}_2\text{BH}_4$  0.1 M solution was added for reducing the Ru from ions to metallic form for 3 hours (Fig. 3).

After that, the membrane was washed with distilled water and dried at  $80^\circ\text{C}$ . Three different commercial PES membranes (pore sizes of 50, 220 and 800 nm) were modified by different UV light exposure, from 5 to 30 min. The modified membranes were then characterized by SEM analysis and the Ru was quantified. The catalytic membrane with an initial pore size of 220 nm was selected to perform furfural hydrogenation tests. In order to evaluate the effective presence of the acrylic layer and the Ru content on the PES membrane, different characterisation techniques were employed (ESI $^\dagger$ ). The FTIR analysis was used for measuring the effectiveness of UV grafting, with the acrylic acid polymerization promoted by UV in the presence of compounds such as *N,N*-methylenebisacrylamide and hydroxybenzophenone. Fig. 4 shows the mid IR spectrum of a modified and unmodified PES membrane with an initial pore size of 50 nm. The presence of acrylic acid on the membrane is highlighted by the peaks at 1720, 1620 and about  $1100\text{ cm}^{-1}$ . These peaks represent the stretching of  $\text{C}=\text{O}$ ,  $\text{C}=\text{C}$  and  $=\text{C}-\text{O}$  bonds. The different time periods of exposure to UV light resulted in different polymerization grades of acrylic acid on the membrane. The presence of the acrylic layer led to the loading of different amounts of Ru on the membrane and different transport phenomena. The morphological changes in the membrane and the formation of the active layer were evaluated by SEM (see Fig. 5).

A longer UV light exposure involved a larger absorption of energy by the PES membrane, and the presence of photoinitiators led to the dissociation of free radicals with consecutive acrylic monomer addition. Fig. 5 shows the modified PES membranes using different UV light exposure. A thicker acrylic layer was obtained using an UV energy flux of  $4.84\text{ J cm}^{-2}$  ( $20\text{ }\mu\text{m}$ ) rather than  $2.42\text{ J cm}^{-2}$  ( $15\text{ }\mu\text{m}$ ), which is due to a major concentration of free radicals.

The hydrophilic properties of the modified membrane were quantified by the contact angle between the membrane surface

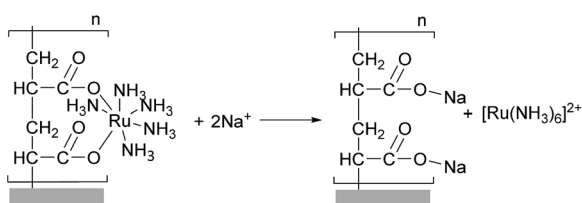


Fig. 3 Redox reaction.

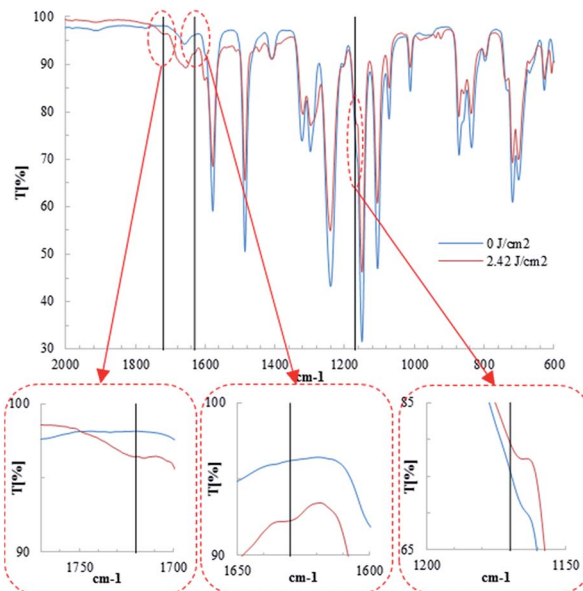
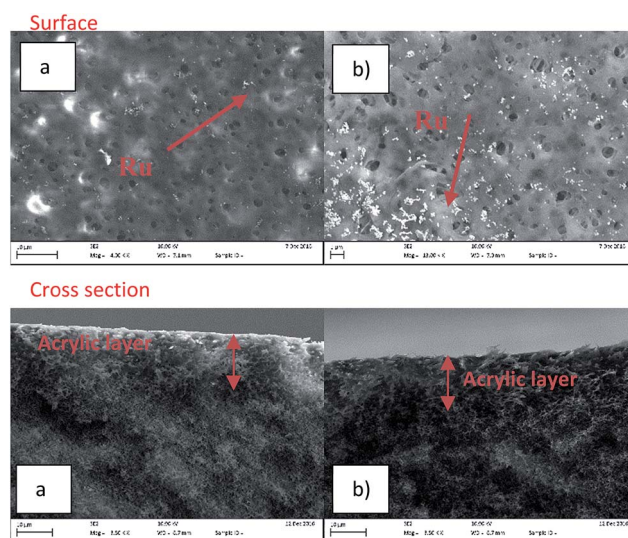


Fig. 4 FTIR spectrum of modified PES.

and a water drop. The measurement confirmed the presence of a coating layer on the PES membrane which resulted in changes in the contact angle, as shown in Fig. 6. For the 50 nm PES membrane and for the bottom layer of the 200 nm PES membrane, there was an increase of the contact angle (decrease of hydrophilic properties). This phenomenon is linked to the presence of Ru nanoparticles on the membrane surface and to their relative orientation.<sup>32,33</sup> The bubble point, pore size distribution and overall porosity were determined, as reported in the ESI, $^\dagger$  before and after the UV light exposure.

The formation of the acrylic layer resulted in a slight decrease of the porosity from 83 to about 77% and from 85 to about 81%, respectively, for the PES membranes with 50 and

Fig. 5 SEM surface and cross-section analyses of the PES-220 nm modified membrane: (a)  $\text{UV} = 2.42\text{ J cm}^{-2}$  and (b)  $\text{UV} = 4.84\text{ J cm}^{-2}$ .

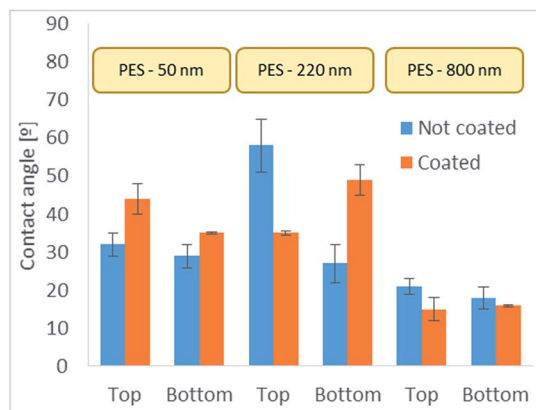


Fig. 6 Contact angle for PES before and after the coating (UV light  $7.26 \text{ J cm}^{-2}$ ).

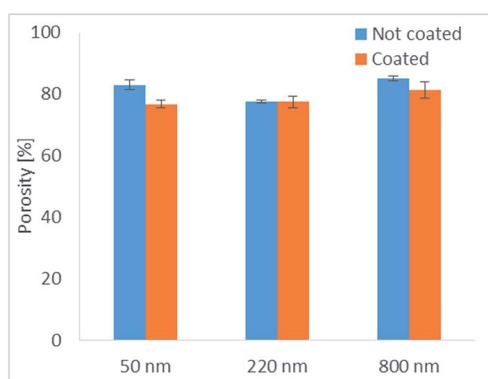


Fig. 7 Porosity of PES before and after the coating (UV light  $7.26 \text{ J cm}^{-2}$ ).

800 nm pore size, as can be seen in Fig. 7. Instead, the porosity did not change for the PES-220 nm. The distribution of the pore size is reported in Table 1, indicating that the presence of the coating layer has no significant effect on the pore size for the PES-50 and 220 nm, while it has the contrary effect on the PES-800 nm. In order to study the effect of acrylic acid and Ru doping on the mechanical properties of the PES membrane structure, the tensile stress was analysed by calculating the Young's modulus and the elongation at break, which resulted to be in the range of  $\approx 150\text{--}250 \text{ N mm}^{-2}$  and 17–32%, respectively. Fig. 8 shows a considerable increase of the Young's modulus

after the coating of the membrane PES-220 nm, while it was almost unchanged for the PES-50 nm and diminished after the coating of the 800 nm PES membrane.

This different behaviour can be attributed to the different morphological structures of the pristine PES membranes, symmetric for the 50 and 220 nm ones and asymmetric for the 800 nm one.

The PES-220 nm also presented an increase of the elongation at break compared to the other two membranes that showed a decrease of the elongation at break after treatment (Fig. 9). The Young's modulus and the elongation break results have been used to assess how the mechanical membrane structure changed after the coating. The high values of Young's modulus for 50 and 220 nm membranes indicate a better resistance to deformation from stress, therefore resulting in a more rigid structure. The elongation at break instead indicates how the membrane absorbs deformation without breaking. For the 50 and 800 nm membranes there was a clear ductility reduction after the coating.

The inductively coupled plasma optical emission spectrometry (ICP-EOS) analysis was used to determine the Ru content loaded on the coated PES membranes with different pore sizes. Fig. 10 shows the concentration of Ru for the tested membranes: 50, 200 and 800 nm. A constant Ru content of about  $9 \mu\text{g cm}^{-2}$  was detected for the PES membranes with a pore size of 800 nm at different UV energies supplied (depending on the UV exposure time). An increase of Ru concentration on the PES membrane surface was noted for the PES membrane with a pore size of 220 nm, with about  $15 \mu\text{g cm}^{-2}$  for the maximum exposure time of UV light (corresponding to the maximum energy used).

An unusual trend was instead observed for the PES-50 nm, with an initial decrease in the amount of Ru deposited on the membrane up to an energy flux of about  $10 \text{ J cm}^{-2}$  and an increase in the amount of the metal deposited at longer UV exposure times up to  $15 \mu\text{g cm}^{-2}$ . From the SEM analysis (see Fig. S2†), it is possible to note that for energy flux lower than  $9.69 \text{ J cm}^{-2}$  (intermediate UV exposure time), the pore sizes on the membrane surface are relatively larger compared to those obtained with longer UV exposure times. For the longest UV exposure time, corresponding to an energy flux of  $14.53 \text{ J cm}^{-2}$ , the Ru content on the modified membrane was almost equal to that obtained for an exposure of  $2.42 \text{ J cm}^{-2}$ , but the pore size distribution was different, five times bigger for the lower energy flux. This difference was caused by the different exposure of UV

Table 1 Bubble point, pore size and maximum pore size distribution for PES before and after the coating (UV light  $7.26 \text{ J cm}^{-2}$ )

Membrane	Bubble point [bar]	Mean flow pore diameter [nm]	Diameter at maximum pore size distribution [nm]
PES-50 nm not coated	1.55	120	70
PES-50 nm coated	0.78	110	72
PES-220 nm not coated	1.14	280	240
PES-220 nm coated	0.62	240	220
PES-800 nm not coated	0.51	850	740
PES-800 nm coated	0.54	770	700

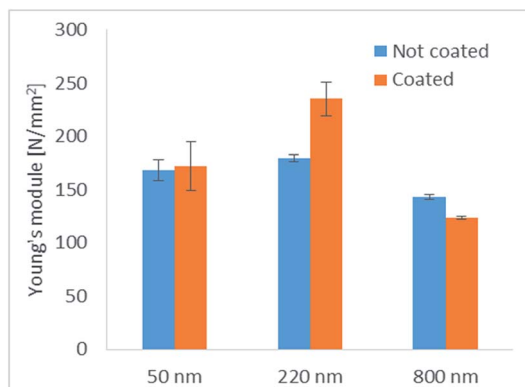


Fig. 8 Young's modulus before and after the coating (UV light  $7.26 \text{ J cm}^{-2}$ ).

light. The increased number of free radicals produced at high energy flux influenced the amount of acrylic deposited and thus the final membrane structure. The pore size reflects the capacity of the membrane to work as a contactor among the phases. Small pore sizes increase the mass transfer resistance of the liquid phase, with consequently reduced contact of the organics in the liquid with the active layer. On the contrary, large pore sizes lead to short contact in the reaction system (liquid/catalyst/gas), and thus a low conversion. The PES-220 nm modified membrane showed an intermediate pore size (maximum pore size distribution of 240 nm). More specific analyses were conducted for the Ru NPs on the PES membrane by Transmission Electron Microscopy (TEM) and X-ray photoelectron spectroscopy (XPS).

The surface composition of the Ru-PES membrane was studied using an XPS technique, as shown in Fig. 11a. The survey-scan XPS spectrum shows all the framework elements of the Ru-PES membrane, which is in agreement with the SEM-EDS data. The high-resolution XPS spectrum shown in Fig. 11b shows two significant bands at 284.2 and 280.6 eV, which can be readily assigned to Ru(0) and Ru oxide, respectively.<sup>34</sup> The presence of Ru oxide can be attributed to Ru

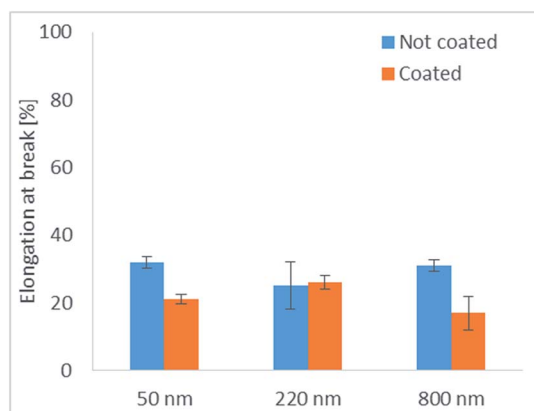


Fig. 9 Elongation at break before and after the coating (UV light  $7.26 \text{ J cm}^{-2}$ ).

oxidation during the sample preparation for the XPS analysis.<sup>35</sup> TEM images show the internal structure of the uncoated and coated active layers of Ru-PES membranes. As shown in Fig. 12, in all cases the presence of Ru nanoparticles is clearly visible, and the coating is homogeneous. In respect to the unmodified membranes, the coated membranes present a thin darker (electron dense) Ru-rich part of the skin and penetration of the Ru nanoparticles into the pores of the support, according to pore size and porosity measurements. Energy-dispersive X-ray analysis was also performed, using the coated and uncoated membranes. The spectra demonstrate that the coated membranes are rich in ruthenium. The additional peaks belong to copper used for TEM grids.

In order to evaluate its activity, once characterised, the PES 220 nm modified membrane (UV light grafting at  $7.26 \text{ J cm}^{-2}$ )

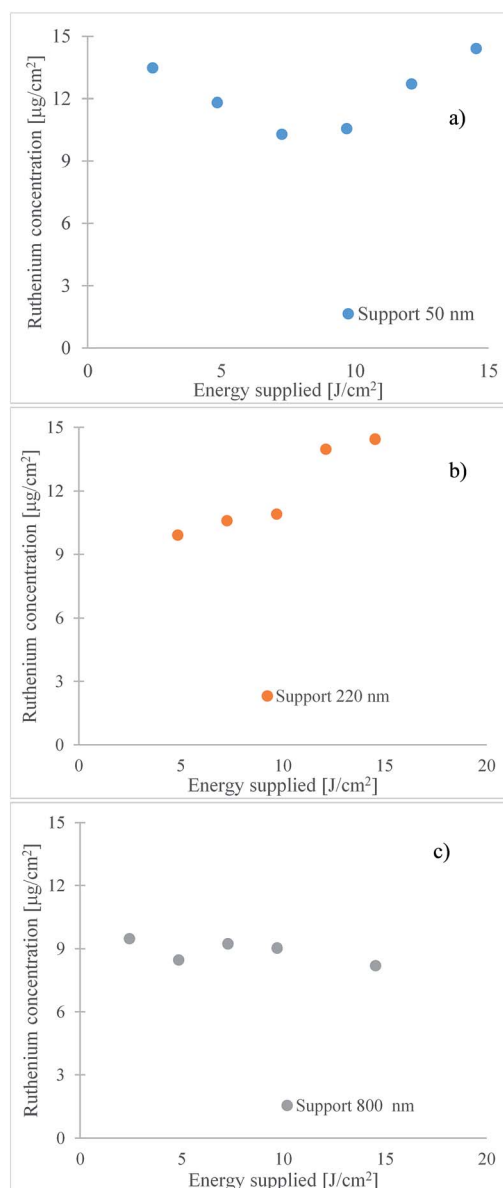


Fig. 10 ICP analysis of modified (a) PES-50 nm, (b) PES-220 nm and (c) PES-800 nm.

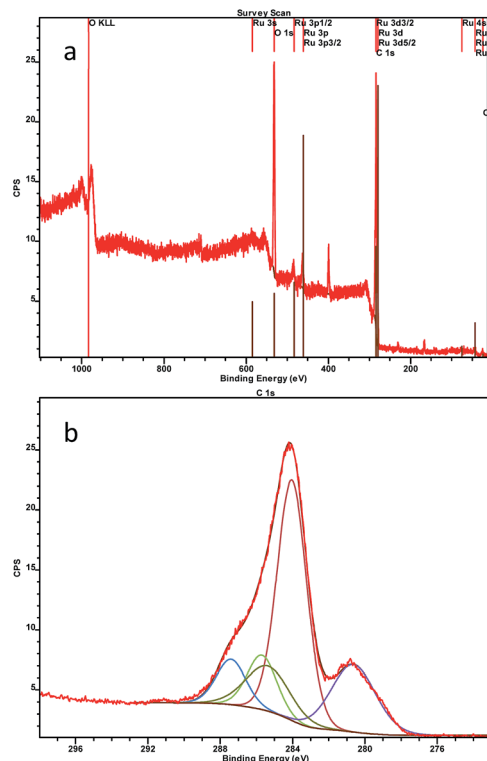


Fig. 11 (a) XPS spectrum of Ru–PES–220 nm and (b) the Ru 3d XPS spectrum of Ru–PES–220 nm.

was tested for the hydrogenation of furfural. The test was carried out in duplicate at 70 °C with a pressure of 7 bar in the gas and liquid zones, a liquid flow rate of 0.497 mL min<sup>-1</sup>, a water feed with 5 wt% furfural and a hydrogen/furfural molar ratio of 1.

For a complete evaluation and comparison with previous studies, the conversion of furfural, the selectivity for the products (i-compound) and the turn over frequency (TOF) have been defined as:

$$x = \frac{\text{Furfural}_{\text{in}} - \text{Furfural}_{\text{out}}}{\text{Furfural}_{\text{in}}} \Bigg|_{\text{molar}} \times 100 [=] \% \quad (1)$$

$$S_i = \frac{\text{i-compound}_{\text{out}}}{\text{Furfural}_{\text{in}} - \text{Furfural}_{\text{out}}} \Bigg|_{\text{molar}} \times 100 [=] \% \quad (2)$$

$$\text{TOF} = \frac{\text{mole of furfural reacted}}{\text{mole of catalyst} \times \text{reaction time}} [=] \text{h}^{-1} \quad (3)$$

Among the potential reaction products reported in Fig. 1, only furfuryl alcohol was detected under the tested conditions (selectivity >99%), with a furfural conversion of 26% after 30 minutes. The conversion and selectivity remained constant for 4 hours. Fig. 13 shows the conversion of furfural for the whole reaction test, where the conversion achieved the steady state condition after 30 min. After 4 h, the conversion of furfural decreased to 17%. A potential contribution to the furfural conversion from homogeneous reactions in the absence of

a catalyst under the studied conditions was excluded *a priori* based on previous assessments. Chen *et al.*<sup>14</sup> did not observe any conversion (less than 1%) at 10 bar and 100 °C without a catalyst.

Moreover, Sanna *et al.*,<sup>4</sup> who investigated the homogeneous (without the presence of a catalyst) continuous flow hydrogenation of furfural at 125 °C and 51 bar H<sub>2</sub> for 36 h, did not observe any change in the furfural concentration at 125 °C.

In order to compare the hydrogenation reaction of furfural with previous studies, the operating conditions, conversion of furfural, product selectivity and TOF present in the literature, are summarized in Table 2.

Since all the previous studies were carried out using batch reactors, similar process conditions can be used to generally compare a PBR reactor *vs.* a CMR. However, a precise comparison of the catalyst properties is difficult due to the different reactor set-ups and hence the use of TOF should be preferred. In eqn (3), the TOF represents the reactant converted per catalyst mole per unit time (typically the second), with the number being a function of the operating conditions. Analysing the TOFs obtained in the available studies on furfural hydrogenation, the highest value of 48 000 h<sup>-1</sup> was obtained in this work, mainly due to different factors: (i) the high hydrogenation activity of Ru at low temperature; (ii) a good stability of Ru in the aqueous phase and (iii) the high hydrogenation selectivity towards the carbonyl group.<sup>16,18,19</sup> Ru catalysts are widely used for hydrotreating biomass-derived substrates at low temperatures.<sup>34</sup> Tan *et al.*<sup>35</sup> studied the Ru activity on different supports for the hydrogenation of levulinic acid to  $\gamma$ -valerolactone from -10 to 100 °C, with a complete selectivity in  $\gamma$ -valerolactone and a conversion of levulinic acid of about 70 and 100%, respectively. (iv) The enhanced contact between the H<sub>2</sub> and the Ru active sites due to the reduced mass transfer limitation<sup>36</sup> in the presence of the modified PES membrane. Under the studied conditions, the presence of three phases is due to a series of mass transfer limitations, where the main limitation step is represented by the hydrogen absorption to the catalyst surface. A method to improve the driving force of the solubility process is increasing the pressure, very common for hydrogenation reactions in the liquid phase, or the enhancement of the contact surface area between the liquid and gas phase. For a PBR, the contact surface area is about 100 m<sup>2</sup> per m<sup>3</sup> of the reactor, while the contact surface area is in the order of 1500–7000 m<sup>2</sup> per m<sup>3</sup> of module for hollow fiber membranes.<sup>37,38</sup> PES was mainly used as an enhanced contactor because of its chemical resistivity in the presence of furfural under the used conditions. Since H<sub>2</sub> in the gas phase has low solubility in the other phase, a higher surface area contact between these phases decreases the need for higher pressure that could have been applied to less soluble components. Moreover, supplying H<sub>2</sub> through a porous membrane allowed the hydrogen to be adsorbed directly onto the Ru surface, and partly solubilised in the liquid phase. The catalytic MR favoured the reaction in terms of TOF; 48 000 moles of furfural have been converted in 1 hour by using 1 mol of Ru catalyst. The conversion of furfural was obtained to be about 26%, a value that is lower than some data reported in the literature, but reasonable if the low ratio of hydrogen/furfural

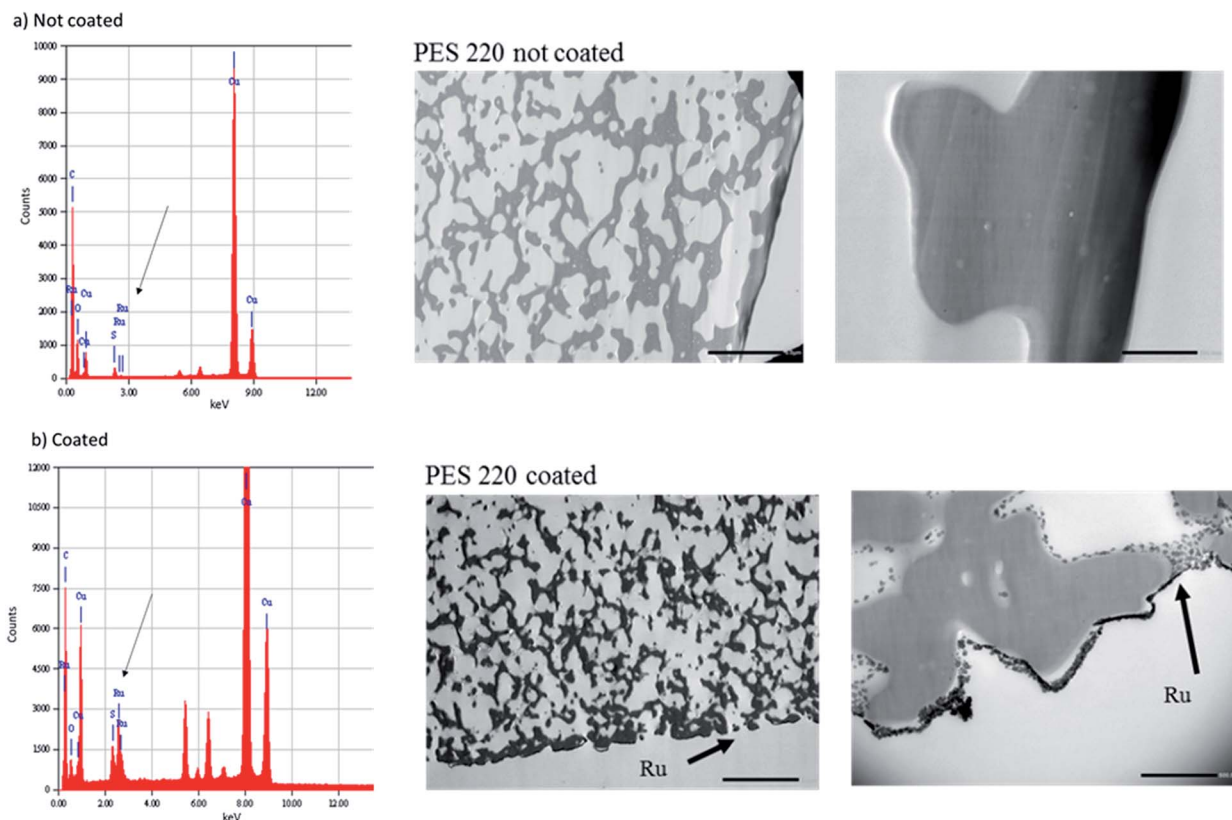


Fig. 12 TEM and EDX analysis of the PES-220 nm membrane (a) not coated and (b) coated (magnification  $\times 2000$  and  $\times 20k$ , scale bar: left,  $5\mu\text{m}$ ; right,  $500\text{ nm}$ ).

(1 : 1) and the fact that only about  $780\ \mu\text{g}$  (2–3 orders of magnitude less than the literature data) of Ru was loaded onto the membrane are considered. Moreover, it has to be stressed that the residence time of the reactants in the membrane layer was very low, at about 1 s, compared to typical residence times  $> 1$  hour in PBRs. For comparison, Nakagawa *et al.*<sup>16</sup> reported a similar conversion (14%) using 2% Pd and 2% Ru on silica with 49% selectivity on furfuryl alcohol after 1 h, but a much higher pressure (80 bar) and  $\text{H}_2$  : furfural molar ratio (125) were used, resulting in a TOF of 337. In the same study and under the

same conditions, 4% Ir/SiO<sub>2</sub> was the most selective to FOL (96%) with a conversion of 14% and a TOF of 67. Fang *et al.*<sup>18</sup> loaded different amounts of Ru nanoparticles, from 1 to 5 wt%, on an acidic MOF material (MIL-101) obtaining a total conversion of furfural at 160 °C and 40 bar and in the presence of 3 wt% Ru/MIL-101, but with a furfuryl alcohol selectivity of only 1%. A complete conversion and selectivity to furfuryl alcohol was obtained by Yang *et al.*<sup>19</sup> at 20 °C and 5 bar in the presence of Ru on an aluminium-based MOF (Al-MIL-53-BDC). However, the TOF in this case was  $21\ \text{h}^{-1}$ , indicating that a large amount of catalyst was used for converting furfural (to convert  $21\ \text{mol h}^{-1}$  of furfural,  $101.7\ \text{g}$  of Ru was used, which corresponds to 3.5 kg of 2.9 wt% Ru/Al-MIL-53-BDC). Chen *et al.*<sup>14</sup> also achieved a 99% selectivity to FOL at a comparable temperature (80 °C) and pressure (10 bar) with 32% conversion and a TOF of 120 using 5% Pt on g-C<sub>3</sub>N<sub>4</sub> nanosheets, but with a  $\text{H}_2$  : furfural molar ratio of 2. In order to improve the furfural conversion, other reaction tests were carried out at the same temperature and reaction pressure, but varying the  $\text{H}_2$ /furfural feed molar ratio to 4 : 1. A maximum furfural conversion of 21% was obtained after 1 hour with a virtually complete selectivity to tetrahydro-furfuryl alcohol. This can be explained by the complete hydrogenation of the heterocyclic ring due to the  $\text{H}_2$  excess. Moreover, the absence of tetrahydrofurfural among the products indicates that an increase of  $\text{H}_2$  favoured further hydrogenation of furfuryl-alcohol to tetrahydrofurfuryl alcohol,

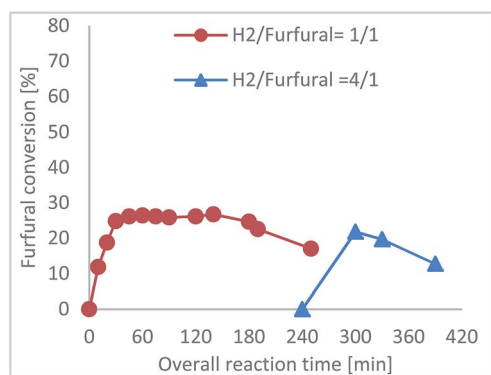


Fig. 13 Furfural conversion vs. time and Ru content before and after the reaction test.

Table 2 Hydrogenation of furfural<sup>a</sup>

Catalyst	Operating conditions					Performance parameters							Ref.
	Solvent	Reactor	Reaction/ resident time	Temperature [°C]	Pressure [bar]	H <sub>2</sub> /furfural molar ratio [–]	Conversion [%]	Selectivity [%]					
								THFA	FOL	THF	Others		
2 wt% Pd/SiO <sub>2</sub>	H <sub>2</sub> O	Batch	1	2	80	125	25	19	69	7	5	21	16
2 wt% Pd/SiO <sub>2</sub>	H <sub>2</sub> O	Batch	1	2	80	125	63	27	33	28	13	53	16
2–2 wt% Pd–Ir/SiO <sub>2</sub>	H <sub>2</sub> O	Batch	1	2	80	125	67	31	47	19	3	1690	16
2–2 wt% Pd–Ru/SiO <sub>2</sub>	H <sub>2</sub> O	Batch	1	2	80	125	14	23	49	20	8	337	16
2–2 wt% Pd–Rh/SiO <sub>2</sub>	H <sub>2</sub> O	Batch	1	2	80	125	5.7	13	77	3	7	137	16
2–2 wt% Pd–Pt/SiO <sub>2</sub>	H <sub>2</sub> O	Batch	1	2	80	125	2.5	5	79	<1	16	63	16
4 wt% Ir/SiO <sub>2</sub>	H <sub>2</sub> O	Batch	1	2	80	125	14	<1	96	<1	4	67	16
2 wt% Pd/SiO <sub>2</sub> 2 wt% Ir/SiO <sub>2</sub>	H <sub>2</sub> O	Batch	1	2	80	125	26	10	85	1	4	262	16
3–1 wt% Pd–Ir/SiO <sub>2</sub>	H <sub>2</sub> O	Batch	1	2	80	125	30	27	47	21	5	522	16
1–3 wt% Pd–Ir/SiO <sub>2</sub>	H <sub>2</sub> O	Batch	1	2	80	125	61	19	67	11	3	2783	16
2–2 wt% Pd–Ir/SiO <sub>2</sub>	H <sub>2</sub> O	Batch	2	2	80	125	99	63	16	20	2	1250	16
2–2 wt% Pd–Ir/SiO <sub>2</sub>	H <sub>2</sub> O	Batch	4	2	80	125	>99	80	<1	18	1	625	16
2–2 wt% Pd–Ir/SiO <sub>2</sub>	H <sub>2</sub> O	Batch	6	2	80	125	>99	80	<1	18	2	415	16
2–2 wt% Pd–Ir/SiO <sub>2</sub>	H <sub>2</sub> O	Batch	6	2	80	125	>99	91	<1	6	4	83	16
2–2 wt% Pd–Ir/SiO <sub>2</sub>	H <sub>2</sub> O	Batch	6	2	80	125	>99	94	<1	1	5	28	16
Ir–ReO <sub>x</sub> /SiO <sub>2</sub>	H <sub>2</sub> O	Batch	8	40	60	1370	>99	0.5	96.9	n/a	2.6	22	17
Rh (0.66)–Ir–ReO <sub>x</sub> /SiO <sub>2</sub>	H <sub>2</sub> O	Batch	8	40	60	1370	>99	58.2	14.4	n/a	27.4	20	17
Pd (0.66)–Ir–ReO <sub>x</sub> /SiO <sub>2</sub>	H <sub>2</sub> O	Batch	8	40	60	1370	>99	66.8	0	n/a	33.2	20	17
Rh (0.66)–Ir/SiO <sub>2</sub> + Ir–ReO <sub>x</sub> /SiO <sub>2</sub>	H <sub>2</sub> O	Batch	8	40	60	1370	>99	6.6	86.6	n/a	6.8	15	17
Rh (0.66)–ReO <sub>x</sub> /SiO <sub>2</sub> + Ir–ReO <sub>x</sub> /SiO <sub>2</sub>	H <sub>2</sub> O	Batch	8	40	60	1370	>99	21.3	55.7	n/a	23	13	17
Pd (0.66)/SiO <sub>2</sub> + Ir–ReO <sub>x</sub> /SiO <sub>2</sub>	H <sub>2</sub> O	Batch	8	40	60	1370	>99	1.9	81.7	n/a	16.4	20	17
5% Pt@CN	H <sub>2</sub> O	Batch	5	100	10	2	60.9	n/a	>99	n/a	n/a	45	14
0.5% Pt@TECN	H <sub>2</sub> O	Batch	5	100	10	2	32.1	n/a	>99	n/a	n/a	242	14
1% Pt@TECN	H <sub>2</sub> O	Batch	5	100	10	2	49.4	n/a	>99	n/a	n/a	186	14
2.5% Pt@TECN	H <sub>2</sub> O	Batch	5	100	10	2	95.9	n/a	>99	n/a	n/a	145	14
5% Pt@TECN	H <sub>2</sub> O	Batch	5	100	10	2	>99	n/a	>99	n/a	n/a	75	14
5% Pt@TECN	H <sub>2</sub> O	Batch	1	80	10	2.11	31.8	n/a	>99	n/a	n/a	120	14
5% Pt@TECN	H <sub>2</sub> O	Batch	1	100	10	2	90.3	n/a	>99	n/a	n/a	340	14
5% Pt@TECN	H <sub>2</sub> O	Batch	1	120	10	1	90.5	n/a	>99	n/a	n/a	341	14
5% Pt@TECN	H <sub>2</sub> O	Batch	1	100	5	1	61.2	n/a	>99	n/a	n/a	231	14
5% Pt@TECN	H <sub>2</sub> O	Batch	1	100	20	2.5	98.0	n/a	>99	n/a	n/a	369	14
1 wt% Ru/MIL-101	H <sub>2</sub> O	Batch	2.5	160	40	2.25	46	n/a	22	n/a	n/a	n/a	18
2 wt% Ru/MIL-101	H <sub>2</sub> O	Batch	2.5	160	40	2.25	93	n/a	16	n/a	n/a	n/a	18
3 wt% Ru/MIL-101	H <sub>2</sub> O	Batch	2.5	160	40	2.25	>99	n/a	1	n/a	n/a	n/a	18
4 wt% Ru/MIL-101	H <sub>2</sub> O	Batch	2.5	160	40	2.25	95	n/a	2	n/a	n/a	n/a	18
5 wt% Ru/MIL-101	H <sub>2</sub> O	Batch	2.5	160	40	2.25	70	n/a	1	n/a	n/a	n/a	18
3 wt% Ru/C	H <sub>2</sub> O	Batch	2.5	160	40	2.25	72	n/a	46	n/a	n/a	n/a	18
2.9% Ru/Al-MIL-53-BDC 25	H <sub>2</sub> O	Batch	1	20	5	1.81 × 10 <sup>6</sup>	12	n/a	>99.9	n/a	n/a	20	19
2.9% Ru/Al-MIL-53-BDC	H <sub>2</sub> O	Batch	1	20	5	1.81 × 10 <sup>6</sup>	21	n/a	>99.9	n/a	n/a	18	19
2.9% Ru/Al-MIL-53-BDC	H <sub>2</sub> O	Batch	2	20	5	1.81 × 10 <sup>6</sup>	100	n/a	>99.9	n/a	n/a	21	19
3.0% Ru/Al-MIL-53-ADP	H <sub>2</sub> O	Batch	1	20	5	1.81 × 10 <sup>6</sup>	3.0	n/a	>99.9	n/a	n/a	4.9	19

Table 2 (Contd.)

Catalyst	Operating conditions					Performance parameters							Ref.	
	Solvent	Reactor	Reaction/ resident time	Temperature [°C]	Pressure [bar]	H <sub>2</sub> /furfural molar ratio [–]	Conversion [%]	Selectivity [%]				TOF [h <sup>-1</sup> ]		
								THFA	FOL	THF	Others			
3.0% Ru/Al-MIL-53-ADP	H <sub>2</sub> O	Batch	1	20	5	1.81 × 10 <sup>6</sup>	5.0	n/a	>99.9	n/a	n/a	n/a	4.1	19
3.0% Ru/Al-MIL-53-ADP	H <sub>2</sub> O	Batch	2	20	5	1.81 × 10 <sup>6</sup>	44	n/a	>99.9	n/a	n/a	n/a	8.9	19
10.9 μg cm <sup>-2</sup> Ru-PES <sup>b</sup>	H <sub>2</sub> O	MR	3.13 × 10 <sup>-4c</sup>	70	7	1	26.13	n/a	>99	n/a	n/a	n/a	4.8 × 10 <sup>4</sup>	This work
10.9 μg cm <sup>-2</sup> Ru-PES <sup>b</sup>	H <sub>2</sub> O	MR	3.13 × 10 <sup>-4c</sup>	70	7	1	20.83	>99	n/a	n/a	n/a	n/a	4 × 10 <sup>4</sup>	This work

<sup>a</sup> THFA = tetrahydrofurfuryl alcohol, FOL = furfuryl alcohol, THF = tetrahydro furfural. <sup>b</sup> Corresponding at 0.080 μg Ru/g PES. <sup>c</sup> Calculated as: reaction volume (equal to membrane volume 6 cm × 12 cm × 130 μm)/overall liquid flow rate (0.497 mL min<sup>-1</sup>).

rather than the formation of tetrahydrofurfural and then its hydrogenation to tetrahydrofurfuryl alcohol, as shown in Fig. 1.

After 150 min from the beginning of the 4 : 1 test, the furfural conversion was reduced to 12%, suggesting that the modified Ru-PES membrane was not stable for the furfural hydrogenation. As can be seen in Fig. 11, the furfural conversion was relatively stable for the first 3 h and then declined to 12% after 6.5 h. To understand the reason for the decreased conversion, the presence of Ru in both (i) the membrane (before and after the experiments) and (ii) the product-solutions was analysed.

The Ru concentration was detected in the product stream in the whole experimental campaign by ICP-EOS and GC-MS analyses, as shown in Fig. 14.

The highest Ru concentration of 40 μg L<sup>-1</sup> was found in the product solution after 30 min, while only half of that concentration (18 μg L<sup>-1</sup>) was in the product after 180 min. At the same time, the GC-MS data did not show the presence of the Ru-Acrylic acid (AA) residue in the product solution. Instead, the Ru-AA residue started appearing from the product sampled after 240 min as shown in Fig. 14.

This suggests that the large presence of Ru in the product after 30 min (about 50% of Ru lost in solution) is most likely related to the removal of “Ru metal clusters” not bonded to the AA that were not removed by the water pre-washing step under ambient conditions. This explains the stability of the catalytic membrane in the first three hours, while the appearance of the Ru-AA residue from the fourth hour suggests that the active layer (acrylic monomer and Ru) was also partially removed in the liquid phase, so that a more resistant metal support rather than acrylic acid would need to be used for the furfural hydrogenation process. Moreover, from the TEM image after the hydrogenation test (Fig. 15), it is possible to see the presence of Ru on the membrane, which appears to have preserved the homogeneity and dispersion of Ru in the coated layer. However, the EDX confirms that overall, the amount of Ru is lower than that before the hydrogenation test. To further elucidate this, at the end of the hydrogenation tests, the metal on the membrane was

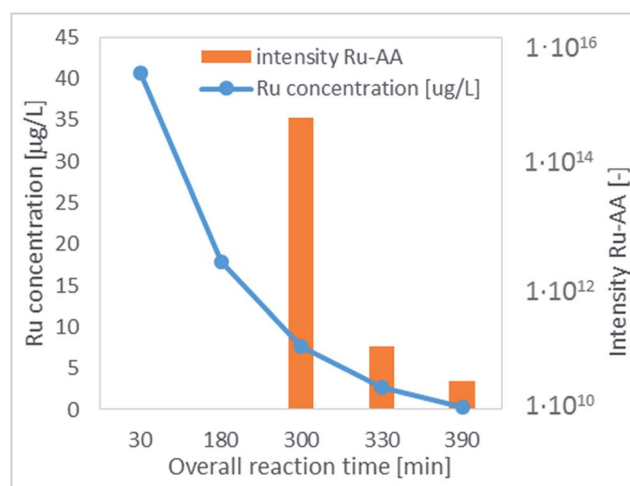


Fig. 14 Ru concentration in product solutions.

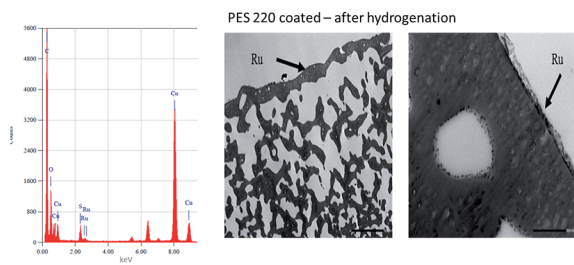


Fig. 15 TEM image after the hydrogenation test (magnification  $\times 2000$  and  $\times 20k$ , scale bar: left,  $5\mu\text{m}$ ; right,  $500\text{ nm}$ ).

quantified before and after the reaction, confirming a decrease from  $10.9\ \mu\text{g m}^{-2}$  to  $5.76\ \mu\text{g m}^{-2}$ , half of which can be linked to the active layer degradation. In conclusion, Ru nanoparticles were added onto the surface of the modified PES membrane using a UV source.

The catalytic membrane was characterized with different techniques in order to evaluate the effective presence of the active layer and the Ru nanoparticles. The membrane with an initial pore size of  $220\ \text{nm}$  and  $10.9\ \mu\text{g cm}^{-2}$  of Ru catalyst was tested for the hydrogenation of furfural under mild conditions ( $7\ \text{bar}$ ,  $70\ ^\circ\text{C}$ ) resulting in  $>99\%$  selectivity towards FOL with a TOF of  $48\ 000\ \text{h}^{-1}$ , when a  $\text{H}_2/\text{furfural}$  molar ratio of  $1:1$  was used. The resulting TOF was considerably higher than those reported in the literature suggesting that the catalytic membrane reactor enhances the catalytic activity of Ru in the selected reaction, while, a  $>99\%$  selectivity to THF was obtained by increasing the  $\text{H}_2/\text{furfural}$  molar ratio to  $4:1$  under the same process conditions. The use of the CMR also resulted in a residence time of the reactants in the membrane layer of less than 2 seconds, compared to a residence time higher than 1 h for conventional PBRs. Therefore, this work indicates that selective hydrogenation of furfural to FOL can be successfully performed using CMRs under mild conditions, but alternative polymeric support materials need to be developed/tested and the recyclability of the catalysts need to be addressed for rendering this pathway commercially viable.

## Conflicts of interest

There are no conflicts to declare.

## Acknowledgements

The authors thank Dr Ida Daniela Perrotta, Department of Biology, Ecology and Earth Sciences (Di.B.E.S.T.), University of Calabria-Arcavacata di Rende, (CS), Italy, for the TEM analysis.

## References

- 1 T. P. Vispute, H. Zhang, A. Sanna, R. Xiao and G. W. Huber, *Science*, 2010, **330**, 1222–1227.
- 2 J. Shi, M. Zhao, Y. Wang, J. Fu, X. Lu and Z. Hou, *J. Mater. Chem. A*, 2016, **4**, 5842–5848.
- 3 H. Bergem, R. Xu, R. C. Brown and G. W. Huber, *Green Chem.*, 2017, **19**, 3252–3262.
- 4 A. Sanna, T. P. Vispute and G. W. Huber, *Appl. Catal., B*, 2015, **165**, 446–456.
- 5 G. Chieffi, C. Giordano, M. Antonietti and D. Esposito, *J. Mater. Chem. A*, 2014, **2**, 11591–11596.
- 6 B. Sarkar, C. Pendem, L. N. S. Konathala, T. Sasaki and R. Bal, *J. Mater. Chem. A*, 2014, **2**, 18398–18404.
- 7 A. Corma, S. Iborra and A. Velty, *Chem. Rev.*, 2007, **107**, 2411–2502.
- 8 H. Li, X. Chen, J. Ren, H. Deng, F. Peng and R. Sun, *Biotechnol. Biofuels*, 2015, **8**, 127.
- 9 D. Santos, U. F. Silva, F. A. Duarte, C. A. Bizzi, E. M. M. Flores and P. A. Mello, *Ultrason. Sonochem.*, 2018, **40**, 81–88.
- 10 K. Kuroda, K. Miyamura, H. Satria, K. Takada, K. Ninomiya and K. Takahashi, *ACS Sustainable Chem. Eng.*, 2016, **4**, 3352–3356.
- 11 H. Deka, M. Misra and A. Mohanty, *Ind. Crops Prod.*, 2013, **41**, 94–101.
- 12 V. V. Pushkarev, N. Musselwhite, K. An, S. Alayoglu and G. A. Somorjai, *Nano Lett.*, 2012, **12**, 5196–5201.
- 13 C. P. Jiménez-Gómez, J. A. Cecilia, I. Márquez-Rodríguez, R. Moreno-Tost, J. Santamaría-González, J. Mérida-Robles and P. Maireles-Torres, *Catal. Today*, 2017, **279**, 327–338.
- 14 X. Chen, L. Zhang, B. Zhang, X. Guo and X. Mu, *Sci. Rep.*, 2016, **6**, 28558.
- 15 M. W. Nolte, A. Saraeian and B. H. Shanks, *Green Chem.*, 2017, **19**, 3654–3664.
- 16 Y. Nakagawa, K. Takada, M. Tamura and K. Tomishige, *ACS Catal.*, 2014, **4**, 2718–2726.
- 17 S. Liu, Y. Amada, M. Tamura, Y. Nakagawa and K. Tomishige, *Catal. Sci. Technol.*, 2014, **4**, 2535–2549.
- 18 R. Fang, H. Liu, R. Luque and Y. Li, *Green Chem.*, 2015, **17**, 4183–4188.
- 19 J. Yang, J. Ma, Q. Yuan, P. Zhang and Y. Guan, *RSC Adv.*, 2016, **6**, 92299–92304.
- 20 Á. O'Driscoll, T. Curtin, W. Y. Hernández, P. Van Der Voort and J. J. Leahy, *Org. Process Res. Dev.*, 2016, **20**, 1917–1929.
- 21 J. Llop Castelbou, K. C. Szeto, W. Barakat, N. Merle, C. Godard, M. Taoufik and C. Claver, *Chem. Commun.*, 2017, **53**, 3261–3264.
- 22 I. Romanenko, M. Lechner, F. Wendler, C. Horenz, C. Streb and F. H. Schacher, *J. Mater. Chem. A*, 2017, **5**, 15789–15796.
- 23 L. Meng, M. Kanezashi, X. Yu and T. Tsuru, *J. Mater. Chem. A*, 2016, **4**, 15316–15319.
- 24 H. Li, A. Caravella and H. Y. Xu, *J. Mater. Chem. A*, 2016, **4**, 14069–14094.
- 25 W. J. Koros, Y. H. Ma and T. Shimidzu, *Pure Appl. Chem.*, 1996, **68**(7), 1479–1489.
- 26 G. Bagnato, A. Iulianelli, A. Vita, C. Italiano, M. Laganà, C. Fabiano, C. Rossi and A. Basile, *Int. J. Membr. Sci. Technol.*, 2015, **2**, 48–56.
- 27 J. P. Stanford, M. C. Soto, P. H. Pfromm and M. E. Rezac, *Catal. Today*, 2016, **268**, 19–28.
- 28 M. Liu, X. Zhu, R. Chen, Q. Liao, H. Feng and L. Li, *Chem. Eng. J.*, 2016, **301**, 35–41.

- 29 E. C. Mengistie, J.-F. Lahitte, #xe7 and ois, *Int. J. Chem. Eng.*, 2017, **2017**, 1–8.
- 30 W.-S. Lee, J.-C. Lee, H.-T. Oh, S.-W. Baek, M. Oh and C.-H. Lee, *Energy*, 2017, **134**, 731–742.
- 31 R. Bernstein, E. Ant3n and M. Ulbricht, *ACS Appl. Mater. Interfaces*, 2012, **4**, 3438–3446.
- 32 D. X. Ye, T. M. Lu and T. Karabacak, *Phys. Rev. Lett.*, 2008, **100**, 256102.
- 33 L. Y. Ng, A. Ahmad and A. W. Mohammad, *Arabian J. Chem.*, 2017, **10**, S1821–S1834.
- 34 H. Wang, S.-J. Lee, M. V. Olarte and A. H. Zacher, *ACS Sustainable Chem. Eng.*, 2016, **4**, 5533–5545.
- 35 J. Tan, J. Cui, X. Cui, T. Deng, X. Li, Y. Zhu and Y. Li, *ACS Catal.*, 2015, **5**, 7379–7384.
- 36 M. D. Wales, L. B. Joos, W. A. Traylor, P. Pfromm and M. Rezac, *Catal. Today*, 2016, **268**, 12–18.
- 37 H. A. Kramers and K. R. Westerterp, *Elements of chemical reactor design and operation*, Netherlands Univ. Press, 1st British edn, 1963, p. 245, Chapman & Hall, ASIN: B0000CLV7S.
- 38 J. C. Crittenden, R. R. Trussell, D. W. Hand, K. J. Howe and G. Tchobanoglous, *Water Treatment: Principles and Design*, 2012.